1 **A combined geomorphological and geophysical approach to characterising**

2 **relict landslide hazard on the Jurassic Escarpments of Great Britain**

3

4 David P. Boon[a,*], Jon E. Chambers[b], Peter R. N. Hobbs[b], Mathew Kirkham[b], Andrew J Merritt[c], Claire

5 Dashwood[b], Catherine Pennington[b], Philip R. Wilby[b]

6 [a] British Geological Survey, Columbus House, Tongwynlais, Cardiff, CF15 7NE, UK.

7 [b] British Geological Survey, Environmental Science Centre, Keyworth, Nottingham, NG12 5GG, UK

8 [c] Plymouth University, Drake Circus, Plymouth, PL4 8AA, UK

9

10 *Corresponding author. Tel: +44 2920 521 962

11 E-mail address: dboon@bgs.ac.uk (D.P. Boon)

12

13

Abstract

15 The Jurassic Escarpment in the North York Moors in Northern Britain has a high density of deep-

16 seated relict landslides but their regional hazard is poorly understood due to a lack of detailed case

17 studies. Investigation of a typical relict landslide at Great Fryup Dale suggests the crop of the Whitby

18 Mudstone Formation is highly susceptible to landslide hazards. The mudstone lithologies along the

19 Escarpment form large multiple rotational failures which break down at an accelerated rate during

20 wetter climates and degrade into extensive frontal mudflows.

21 Geomorphological mapping, high resolution LiDAR imagery, boreholes, and geophysical ERT

22 surveys are deployed in a combined approach to delimit internal architecture of the landslide. Cross

23 sections developed from these data indicate the main movement displaced a bedrock volume of c.

24 1×10^7 m^3 with a maximum depth of rupture of c. 50 m. The mode of failure is strongly controlled by

25 lithology, bedding, joint pattern, and rate of lateral unloading. Dating of buried peats using the AMS

26   method suggests the 10 m thick frontal mudflow complex was last active in the Late Holocene, after

27   c. 2270±30 calendar years BP.

28   Geomorphic mapping and dating work indicates the landslide is dormant, but slope stability

29   modelling suggests the slope is less stable than previously assumed; implying that this and other

30   similar landslides in Britain may become more susceptible to reactivation or extension during future

31   wetter climatic phases. This study shows the value of a multi-technique approach for landslide hazard

32   assessment and to enhance national landslide inventories.

33

34   **Keywords: Jurassic Mudstone; Landslide; LiDAR; ERT.**

35

1 Introduction

37

38   Landslide hazards pose a threat to people and infrastructure worldwide. They are a constraint on land

39   use and can impact on the economy of an affected community (e.g. Jones and Lee, 1994; Schuster and

40   Highland, 2001). However, our ability to assess hazard and risk in slide prone terrain, such as the

41   North York Moors (NYM) region of the UK, and in Polar Regions currently undergoing de-

42   glaciation, is hindered by a lack of knowledge about the magnitude and frequency of events and

43   hillslope processes operating in these settings more generally. This paper provides a baseline

44   reference study for landslide hazards in mudrocks that can be used to calibrate magnitude/frequency

45   estimations for landslide hazard assessments in the region and in similar geological terrain elsewhere.

46   Jurassic mudrocks underlie much of the UK including the North Yorkshire Moors area. These rocks

47   are exposed in coastal slopes which are prone to instability (Jones and Lee, 1994; Fish et al., 2006;

48   Cooper, 2007; Johnson and Fish, 2012) but landslide problems on inland escapement slopes in the

49   NYM region are under-represented in the literature (Senior and Rose, 1994; Waltham and Foster,

2

50   1999; Marsay, 2010; Merritt et al., 2013). Previous geomorphological studies in the region (Fox-

51   Strangways et al., 1885; Gregory, 1962a) did not describe the landslide geology or geomorphology in

52   any great detail. This paper aims to address this knowledge gap.

53   The study focuses on the Mark Nab landslide in Great Fryup Dale, Upper Eskdale (Fig. 1), which is

54   the largest in a cluster of bedrock landslides distributed throughout several of the deep valleys in the

55   north of the region. We combine newly acquired remote-sensing data (LiDAR), ground-based

56   geomorphological mapping, electrical resistivity tomography (ERT), and geotechnical data into a

57   ground model in order to conceptualise the 3D landslide architecture. We also use Accelerator Mass

58   Spectrometry (AMS) dating methods to further develop the movement history. This ground model

59   was then used to develop a deterministic slope stability model to test theories about trigger and

60   preparatory factors that led to the initial failure; including changes in stress and porewater pressure

61   brought about by glacial erosion, glacial de-buttressing, changes in regional groundwater levels and

62   glacial lake development. An assessment of the present stability state of the dormant slope is also

63   presented to provide an indication of the current and future regional hazard posed by relict landslide

64   systems.

65

66 Fig. 1. The Mark Nab landslide on the Jurassic escapement, showing complex landslide morphology.

67 Looking south-west. Photo taken by A. H. Cooper. Copyright BGS/NERC P769517.

68

2. Mark Nab study area

70

2.1. Topography

72 The study area, located at British National Grid reference 471350, 502840 (54.42, -0.90 WGS84),

73 covers a north facing slope on the Jurassic escarpment at the head of Great Fryup Dale (Fig. 2). The

74 foot of the slope lies at c. 150 m above Ordnance Datum (aOD) and rises up over hummocky ground

75 by c. 200 m over a distance of c. 600 m. At the top of the slope, Middle Jurassic bedrock is exposed in

76 the near-vertical cliff that forms the main Jurassic escarpment, above which is an upland moorland

77 plateau which reaches a high point of 432 m aOD on Danby High Moor. The plateau sits at the

78 northern edge of the North York Moors which are fragmented by a series of deep valleys generally

79 orientated south-west north-east. The heads of these valleys are commonly incised by streams fed by

80 runoff from peat covered moorland catchments. Numerous springs issue groundwater along the foot

81 of the escarpment. The streams, such as Great Fryup Beck in 'Dale Head' and Slidney Beck (Fig. 2)

82 then flow north-eastwards into the River Esk which discharges into the North Sea at Whitby. At Great

83 Fryup Dale the lower valley slopes are U-shaped and are typically inclined at c. 20°, but towards the

84 head of the valley (Dale Head) the profile becomes increasingly V-shaped and irregular, due to

85 Holocene fluvial incision and slippage.
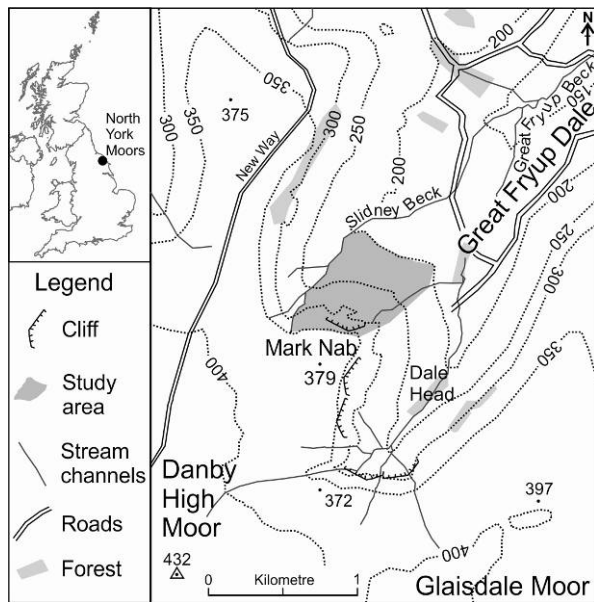
86

87 Fig. 2. Location map of the Mark Nab landslide study site at Great Fryup Dale, North York Moors.

88 Contours and spot heights are in metres above Ordnance Datum. Contains Ordnance Survey data ©

89 Crown copyright and database right 2014.

90

91 *2.2. Bedrock geology*

92 The Great Fryup valley is cut into a bedrock succession of Lower to Middle Jurassic sedimentary

93 rocks comprising units of mudstone, siltstone and sandstone, with subsidiary ironstone bands and

94 limestone beds that together represent subsidence and eventual infilling of the Cleveland Basin (Kent

95 et al., 1980; Holliday et al., 1992; Cox et al., 1999). The valley is positioned on the northern limb of

96 the east-west trending Cleveland Anticline structure. The bedding in the valley is typically near-

97 horizontal but locally dips 1° to 2° to the north, dipping gently out of the slope below Nark Nab.

98 The succession comprises formations of the Lower Jurassic Lias Group, overlain by those of the

99 Middle Jurassic Ravenscar Group. The typical lithologies of this succession are summarised in Table

100 1.

101

102 Table 1. Lithostratigraphic details and thickness of the bedrock sequence exposed in Great Fryup Dale

103 (based on Kent et al., 1980; Howard, 1985; Powell et al, 1992; Young, 1994; Cox et al., 1999; Powell,

5

2010; Barron et al., 2012).

Lithostratigraphy and local thickness			Lithology
Middle Jurassic	Ravenscar Group	Moor Grit Member of the Scalby Formation c. 15 m	Grey medium- to coarse-grained, pebbly, trough cross bedded sandstone, with thin siltstone and mudstone beds. Plant fragments and wood common.
		Scarborough Formation 30 m	Variable lithology: fossiliferous argillaceous limestone, calcareous mudstone, siltstone, and medium-grained sandstone; calcareous concretions and ironstone.
		Cloughton Formation 50-70 m	Laminated grey mudstone and siltstone with yellowish grey, fine- to medium-grained, cross-stratified sandstones and rare thin coals and seatearths.
		Eller Beck Formation 4.5-6 m	Upward-coarsening succession of mudstone (with ironstone concretions), siltstone and fine- to medium-grained sandstone. Sandstone commonly ripple laminated, yellow weathering, bioturbated.
		Saltwick Formation c. 37 m	Grey mudstone, yellow-grey siltstone and fine- to coarse-grained sandstone. Cross stratified, non-bioturbated. Sandstone beds and channel fills. Thin coals, seatearth mudstone and nodular ironstone, plant fragments, rootlets common in some beds.
		Dogger Formation 7-8 m	2 to 3 m thick beds of deep-red poorly sorted coarse-grained sandstone, with chamositic (green) ooliths and scattered rounded granules and pebbles.
Lower Jurassic	Lias Group	Blea Wyke Sandstone Formation c. 5 m	Micaceous, fine-grained sandstones: grey-weathering and argillaceous in lower part, yellow-weathering and silty in the upper part.
		Whitby Mudstone Formation Locally c. 90 m	Medium and dark grey fossiliferous mudstone and siltstone, laminated and bituminous in part, with this siltstone or silty mudstone beds. Sporadic thin sideritic and calcareous beds, limestone and phosphatic nodules and concretions. Pyritic.
		Cleveland Ironstone	Grey silt-laminated mudstone with up to six 0.1 to 0.3 m thick interbeds of hard, fossiliferous, ooidal ironstone

		Formation Up to c. 25 m	(siderite and berthierine).
		Staithes Sandstone Formation Up to c.30 m	Silty sandstone with 2 to 4 m thick packages of laminated fine-grained sandstone in the middle and upper parts: typically bioturbated and/or showing wide variety of bedding structures.
		Redcar Mudstone Formation Up to c. 283 m	Grey, fossiliferous, fissile mudstones and siltstones with subordinate thin beds of shelly limestone below, fine-grained carbonate-cemented sandstone above: argillaceous limestone concretions occur thoughout.

105
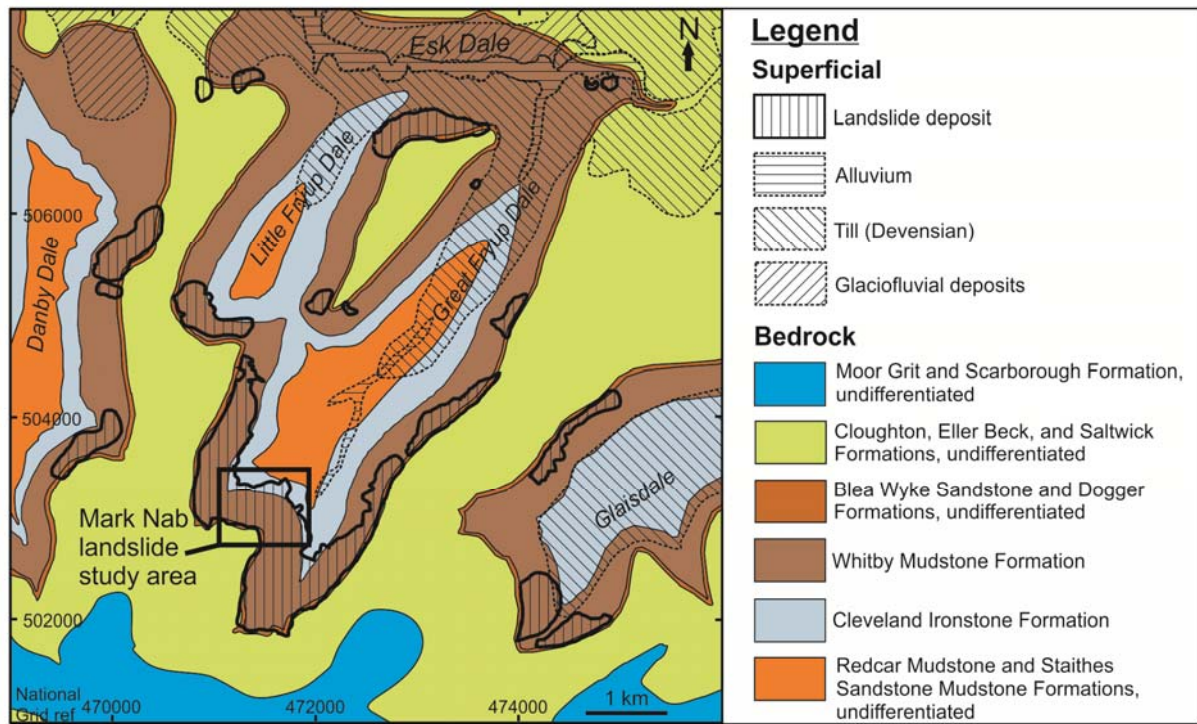
106

107   Fig. 3. Geological map of Great Fryup Dale, adapted from Holliday et al. (1992), Sheet 43 Solid and

108   Drift Edition, with unpublished BGS landslide deposit mapping data. Contains British Geological

109   Survey materials © NERC 2014.

110

111   The overview geological map in Fig. 3 shows that landslide deposits are extensive in Great Fryup

112   Dale and are largely coincident with the Whitby Mudstone Formation (WHB) and Dogger and Blea

Wyke Formations. The Whitby Mudstone Formation is predominantly argillaceous and locally c. 90 m thick, comprising grey to dark grey, finely laminated, fissile, pyritic mudstone and silty mudstone with sporadic thin sideritic and calcareous beds and concretions (Powell, 2010; Table 1). The formation comprises five lithologically distinct Members (Cox et al., 1999) each displaying slightly different geotechnical properties. This subtle variation in physical properties strongly influences landslide mechanism, scale, style and preservation potential across the region and the details of individual member beds is worthy of description and some discussion here. Of particular importance to slope stability is the presence of 'slide-prone horizons' within argillaceous units, as defined by Bromhead and Ibsen (2004), which give rise to bedding controlled failures. The finely laminated (fissile) nature and pyrite content of some beds creates strength anisotropy. The basal unit of the Whitby Mudstone Formation, the Grey Shale Member, consists of c.14 m of pale grey, locally pyritic, silty mudstone with calcareous siderite concretions (Powell, 2010). A change to anoxic conditions are reordered in the overlying Mulgrave Shale Member, which is c. 31 m thick and includes 9–10 m of fissile, finely laminated, bituminous, dark grey mudstone (previously 'Jet Rock') with horizons of calcareous concretions and a thin pyritic limestone at the top (previously 'Top Jet Dogger'), passing up into c. 23 m of fissile, bituminous mudstone with abundant ammonites (formerly 'Bituminous Shales'). The Alum Shale Member above is c. 37 m, comprising a lower soft grey silty (micaceous) mudstone that includes c. 6 m of non-bituminous shale capped by a band of siderite nodules, overlain by c. 15 m of pyritic shale (the main 'Alum Shales'), then 13–20 m of harder shale (formerly 'Cement Shales') that include beds of calcareous nodules (Kent et al., 1980; Powell, 2010). The Middle Jurassic Dogger Formation rests unconformably on the Alum Shales in this part of the Cleveland Basin and the overlying Peak Shale and Fox Cliff Members exposed along the Yorkshire coast near Whitby are absent (Powell, 2010).

Kent et al. (1980) interpreted the overall structural grain of the regions distinct sub-parallel valleys to be the result of basin inversion, uplift, erosion and unloading. This structural history produced a pervasive radial joint pattern which had led to the development of the distinctive radial drainage pattern. In the north of the Moors the predominant N–S structural grain and topography led to the

140   formation of a series of near-parallel north-south orientated valleys, and Great Fryup Dale serves as a

141   fine example of one of these consequent drainage features. Joints are pervasive and laterally and

142   vertically persistent in the sandstone beds that cap the mudstones, and are generally orientated near-

143   parallel to the valley slopes. The presence of these joints, together with occasional faults, reduces the

144   mass strength of the cap rock and Dogger Formation beds in a preferential orientation, and also

145   increases the permeability and storage capacity of these units (creating aquifers). These structural

146   factors, along with the presence of weak horizons, strongly control landslide susceptibility and

147   mechanisms of failure.

148

149   *2.3. Quaternary history*

150   Great Fryup Dale was glaciated through the Devensian and became de-glaciated in late-Devensian

151   times (Jones, 1977; Jones, 1999). During the Last Glacial Maximum (LGM) of Marine Isotope Stage

152   2 (around 18 000 yrs BP), the high ground on the North York Moors remained largely ice free but

153   experienced very severe periglacial conditions (Innes, 1999; Innes et al., 2009; Chiverrall and

154   Thomas, 2010). At this time the valley was probably fully glaciated by a tongue of ice from a glacier

155   in the Esk Valley (Kendall, 1902; Kent et al., 1980; Chiverrell and Thomas, 2010; Murton and

156   Murton, 2011). De-glaciation commenced c. 13 000 yrs BP, in the Late Glacial Interstadial but was

157   interrupted by a brief final cold stage between about 10 800 and 10 400 yrs BP, during the Loch

158   Lomond Stadial (Innes, 1999). Glaciation left patchy deposits of till in the valley floor (Fig. 3) and

159   prolonged periglacial conditions left spreads of periglacial Head deposits across slopes. Holocene

160   rivers cut down through till, deposited alluvium across the valley floor, and cut terraces into the

161   bedrock. Landslide deposits formed in oversteepened valley heads and along valley sides, sometimes

162   blocking stream channels which temporarily diverted river flow. On the hill tops peat deposits cover

163   much of the plateau, which along with some valley slopes to the south (e.g. Rosedale) are peppered

164   with shallow coal and ironstone workings and small mine spoil heaps.

165

3. Slope geomorphology at Mark Nab

The landslide at Mark Nab is c. 700 m long and c. 600 m wide; it covers approximately 0.36 km^2 (Figs. 3 and 4). The crown of the landslide is at an elevation of c. 340 m aOD, and the toe is at c. 190 m aOD. The flanks abut against adjacent landslide deposits to the east and west.

3.1. LiDAR interpretation

Airborne LiDAR data were acquired by the Environment Agency Geomatics Group at a resolution of 0.25 m (flown March 2012). The derived shaded digital terrain model (Fig. 4) was interpreted and main landslide features initially mapped out using a GIS and adopting the descriptive terms from Cruden and Varnes (1996). Based on this mapping and supplementary detailed field-based mapping, three distinct morphological zones (I–III) were identified within the one landslide system:

Zone I – rear scarp with rockfall

Zone II – main body with rotated landslide blocks, block disruption, minor scarps and grabens

Zone III – frontal mudflow complex with concealed block disruption or weathered bedrock

The following section describes the geomorphology of the slope as interpreted from the LiDAR data (Fig. 4).

The average slope angle on the landslide varies widely; a concave near vertical cliff dominates Zone I, whereas slopes of up to 42° are locally present in Zone II. The lower slopes in Zone III are generally smooth and gently undulating with an overall convex form downslope.
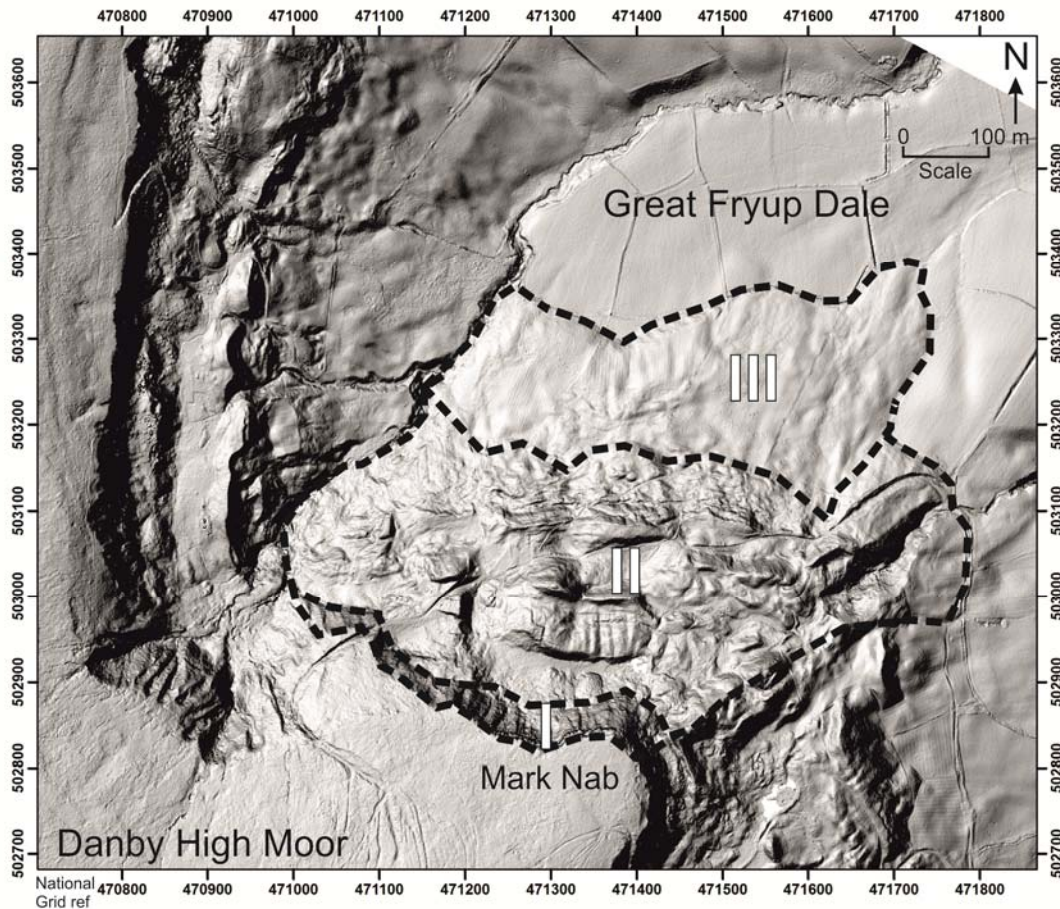
Fig. 4. Use of high-resolution LiDAR. A derived Digital Terrain Model of Great Fryup Dale (0.25 m

x,y, resolution, 0.015 m vertical resolution, flown by Environment Agency 10 March 2012).

Coordinate system is British National Grid. Three main morphological zones (I–III) are defined based

on surface morphology.

3.1.1. Details of Zone I

Zone I contains the rear scarp of the landslide, which is c. 370 m long, up to 40 m high. This feature

forms a sharp crescent shaped cliff separating the sheltered valley from the exposed moorland plateau.

The upper portion of scarp is a near vertical 6 m high cliff exposing thickly bedded gritty sandstone

blocks of the Cloughton Formation (Sycarham Member) and the finer more thinly bedded Eller Beck

Formation below. The rock mass is locally regularly jointed and blocky, with three orthogonal joint

11

197   sets present; oriented ESE, SE and NE. These joints intersect the near-horizontal bedding which

198   daylight in the cliff face. This kinematic geometry favours 'toppling' and 'sliding' modes of failure,

199   and failures typically releasing fairly large (1 to 3 m^3) blocks of sandstone, which have accumulated

200   in a talus cone at the foot of the main scarp, partially filling the surface depression formed by the rear

201   graben.

202   The lower half of the escarpment cliff (main scarp) exposes mudstones and sandstones of the Saltwick

203   Formation. Continued erosion of the cliff has deposited a thin veneer of 'gravelly clay' on the slope

204   which periodically fail in translational debris-rich mud slides also feed fluidised sediment, sometimes

205   via chutes, into the depression below (graben). Several freshwater springs emerge from Sycarham

206   Member along the base of the main sandstone cap, and also from several sandstone channels present

207   within the predominantly silty Saltwick Formation. Erosion by these springs forms small gullies in the

208   backscarp, and fossil gullies are preserved on the eastern most rear landslide block.

209   The western side of the escarpment slope has undergone differential erosion leading to bevelling of

210   the bedrock surface (Cloughton Formation) which has produced a more rounded profile in the east.

211   Above Zone I, at the western end of the main scarp, is a north-west-facing slope facet, with a

212   distinctively smooth, regular, and convex profile which becomes progressively steeper downslope

213   (19–26°). This slope is mantled with at least 2–3 m of soliflucted head deposits composed of stiff grey

214   slightly gravelly, silty, sandy clays with rare rounded pebbles. These pebbles may have been reworked

215   from a pre-Devensian till. This slope is also scattered with large rounded boulders of coarse-sandstone

216   and are notably more deeply weathered than the rockfall blocks from the back scarp. It is most likely

217   that this slope facet is a periglacial 'boulder field' with boulders sourced from the thick sandstone bed

218   that crops out at the crest of the slope (see Fig. 5). Another such 'boulder field' is present on an east-

219   facing slope facet located c. 200 m to the west, on the opposite side of the valley.

220

221   *3.1.2. Details of Zone II*

222   The upper part of Zone II contains a 30 m wide, 200 m long, flat waterlogged depression. This is

223   interpreted as a rear graben that separates the rear scarp from the main body of the landslide. The

224   graben contains 0.5 m of peat over at least 2 m of wet soft silt. A low man-made earth dam (built c.

225   2010) impounds excess surface and spring water in the graben formed depression to supply nearby

226   farms.

227   The middle part of Zone II contains a c. 200 m long area of highly irregular topography characterised

228   by massive blocks, each c. 100 m wide and c. 60 m long, with secondary slope parallel scarps up to

229   20 m high. The highest blocks are capped by a band of resistant ferruginous limestone of the Blea

230   Wyke Member and are composed mostly of Whitby Mudstone Formation mudstone. These beds dip

231   at c. 20° to the south in the rearmost blocks, but the dip increases to up to c. 58° on the frontal blocks.

232   The edges of the main landslide blocks are markedly linear and strike NNE, as can be clearly seen

233   from the LiDAR DTM (Fig. 4). This orientation matches the principal joint set orientation (measured

234   in sandstone exposed in the main cliff above), suggesting an inherent structural control on landslide

235   morphology. Small ponds occur in depressions between the main landslide blocks and are filled by

236   several metres of laminated silt with occasional cobbles (proved by Russian Corer and hand

237   auguring). The topography of the eastern side of Zone II is generally more subdued than the western

238   side following more intense reworking and infilling of topographic depressions by mudflows

239   generated by high amounts of water issuing from the springs and small springs that drain the rear

240   pond.

241   The eastern flank of the main landslide is represented at surface by a c. 150 m long, 15–20 m high

242   scarp feature which forms a linear trough. It is currently occupied by a stream fed by the rear pond

243   and is bounded to the east by a ridge composed of slipped fissile mudstone capped by a red sandstone.

244   The western margin of Zone II represents the western flank; this area of rough ground is characterised

245   by a complex association of morphological features created by a series of superficial shallow multiple

246   landslides formed in the pre-slipped mudstone, similar in style to the lowest part of Zone II. Slope

247   instability in this part of Zone II is primarily driven by toe erosion by Slidney Beck. The course of this

13

248   stream has clearly been obstructed, and likely dammed, by landslide deposits on multiple occasions,

249   and diversion of the stream has carved new channels and fluvial terraces, and proceeded to undercut

250   other suspended landslide deposits.

251   Below the 270 m contour line morphology in Zone II is typically more subdued with 5–10 m high

252   minor scarps and transverse tension cracks that run parallel with the slope. The lowest slopes in Zone

253   II consists solely of mudstone beds (with sandstone absent) which are rotated by up 45° in boreholes 2

254   and 3. Contorted tightly folded beds of mudstone are exposed in a track cutting and stream section at

255   the toe (locations 3–5 in Fig. 5). It is likely that this lower area contains the main slip surface

256   breakout, and although the shear surfaces are masked by superficial slumped mudstone, their surface

257   expression can be traced along a slight rise in ground level.

258

259   *3.1.3. Zone III*

260   Zone III is typically smoother than Zones I and II, with irregular slopes of c. 9–12°. This zone

261   contains the foot and toe of the landslide. This zone is c. 200–300 m long, c. 600 m wide and contains

262   degraded mudflow lobes, peat hollows and some spring lines. The toe area has been artificially

263   drained to improve the quality of the pasture land. The western side has degraded ridge and furrow

264   plough lines which are disturbed above the 245 m contour line where grass pasture gives way to

265   bracken and the ground is crossed by degraded transverse cracks.

266   Below Zone III the ground is very smooth and slopes gently to the north. This area is interpreted to

267   preserve a glacially eroded surface which has later been modified by streams emanating from the toe

268   of the landslide, and diverted around the toes of other landslide masses that have previously dammed

269   Slidney Beck. These stream diversion events have likely caused erosion of the toe, evidenced by a

270   low cliff feature along the western end of the toe.

271

272   *3.2. Geomorphological plan*

273 The morphological features interpreted from the LiDAR were combined with detailed geological field

274 mapping to produce a 1:2 500 scale 'geomorphologic plan' (Fig. 5; as per Anon, 1972; Griffiths,

275 2002; Fell et al., 2008). The plan depicts the key morphological features and geology, with structural

276 data, field localities (numbered locality 1–13), borehole and dynamic penetrations test locations,

277 geophysical survey lines, and lines of cross-section. The Cloughton and Saltwick Formations are

278 exposed in the main back scarp and erosion of these materials contributes to rockfall, mudslides and

279 accumulation of tallus (Loc. 13). On the main body (Zone II) several Whitby Mudstone cored blocks

280 are capped by the more resistant sandstone and limestone beds of the Dogger and Blea Wyke

281 formations. Their lithologically distinctive beds provide key stratigraphic markers across the slipped

282 ground, and their southerly dips and drop in elevation, provide evidence for back rotation of the

283 landslide mass. The extents of these marker beds was mapped out in detail, with structural

284 measurements taken to help model the subsurface structure of the landslide blocks. Periglacial head

285 deposits above and west of the main backscarp are truncated by the rear scarp exposing the non-

286 marine siltstone and mudstones of the Saltwick Formation. This relationship has important

287 implications for the landslide movement history, as discussed later. On the far western flank, Slidney

288 Beck has been diverted around the toe of a secondary landslide deposit shows a cross section through

289 this part of the slope). The scarp of this toe failure truncates the main scarp feature and this provides

290 evidence for erosion-driven reactivation after the main failure, although the relative age of this

291 subsequent failure has not yet been investigated. The steam is currently eroding the river bank at the

292 foot of Zone II, and thereby continues to destabilise the western side of the landslide system. In the

293 upper part of Zone III the sharpness of minor scarps, which define the boundaries of the secondary

294 rotations through 'block disruption' (9 and 10), and tension cracks (11) have become much degraded.

295 The disrupted Whitby Mudstone Formation mudstone slakes fairly readily and has degraded to mud

296 which feeds into flows that supply material to the lower mudflow complex (6) producing a smooth

297 slope profile (7 and 8) across the crop of the Cleveland Ironstone Formation bedrock surface.

298 Contorted and tightly folded beds of mudstone are well exposed in a sunken track (4 and 5) in the

299 eastern toe area. These structures are interpreted as a product of compression related to landsliding,

300　and not the result of tectonic faulting, though these features could also potentially relate to earlier

301　cambering and valley bulging processes which would have preconditioned the slope for failure.

302
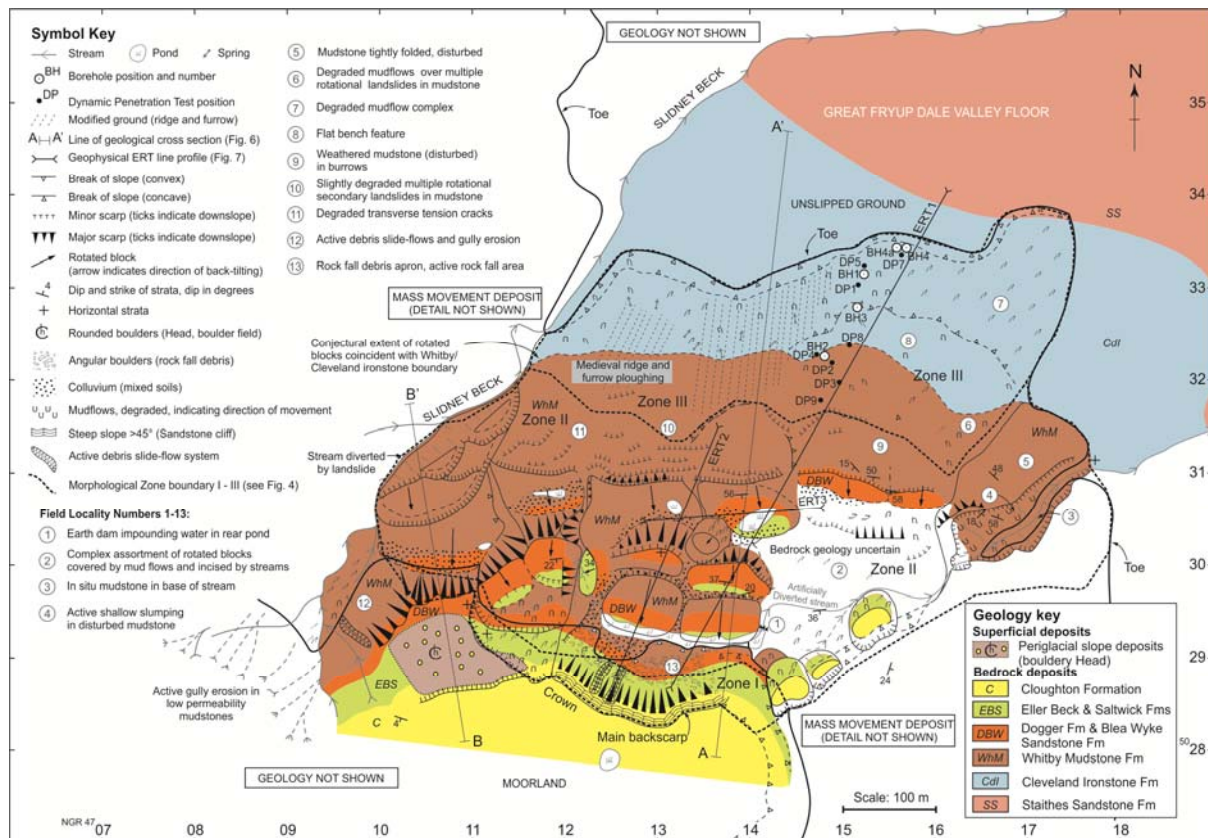
303

304　Fig. 5. Geomorphologic plan of the Mark Nab landslide showing key localities, positions of boreholes

305　(BH1, 2, 3, 4, 4A), dynamic penetration tests, ERT lines (ERT1, 2, 3), geological cross section lines A

306　and B, and relation of surface morphological features to the landslide morphological Zones I–III

307　defined in Fig. 4.

308

4. Subsurface investigations

4.1. Drilling and testing

Five boreholes (1, 2, 3, 4, 4A) were drilled in the foot of the landslide to assess the stratigraphy and to provide ground-truth for the geophysics. The boreholes (BH) were logged to British Standards for Site Investigation (BS5930,1999; BS EN ISO 14688-1 and weathering described according to Anon, 1995). Full logs are presented in Appendix 1and BH locations shown in Fig. 5. The core was sampled in a fresh state for classification tests, including moisture content, bulk density, resistivity and shear strength (unconsolidated undrained for 'peak' values, and consolidated drained for 'residual' values). The BH 4A was a re-drill of BH4 drilled to collect additional samples.. Dynamic Penetrometer (DP) tests were also undertaken to provide correlation of hard and soft zones between boreholes. The DP's were progressed to refusal ($N \geq 60$), terminating within unslipped mudstone or harder ironstone or siderite bands. A standpipe piezometer installed in BH2, located in Zone III, to monitor shallow groundwater levels, and was monitored between March to November 2012 using a *Solnist* level logger and barometric logger at 15 min. intervals. Within the monitoring period the water level fluctuated between 2.8 and 3.5 m below ground surface and was sensitive to antecedent rainfall conditions. It is unlikely that this water level represents the water table across the entire landslide, as groundwater conditions are likely to be complex, and possibly compartmentalised in Zone II due to minor aquifers occurring within individual landslide blocks.

The boreholes in Zone III (BH's 1, 3, 4, and 4A) proved weak mudstone bedrock (Whitby Mudstone Formation) overlain by c. 10 m of soft to firm mottled or laminated clay sediments (mudflows). Borehole 2, located further up slope within Zone II, proved 6 m of rotated mudstone beds interpreted as slipped Whitby Mudstone Formation. Boreholes 4 and 4A, in the toe area, proved several metres of deeply weathered mudstone overlain by stiff gravelly clay (head or till) deposits, and capped by soft clay containing an organic-rich peaty soil horizon between 2.64 and 2.90 m b.g.l. These organic rich horizons, which were dated (see later), are interpreted as a palaeosol that formed in a small depression subsequently buried and preserved by a mudflow event.

335

4.2. Geophysical survey

The Electrical Resistivity Tomography (ERT) technique (Jongmans and Garambois, 2007) was used

to compare subsurface characteristics with surface features and ground-truth from borehole data.

Geophysical surveys were acquired along three lines: ERT Lines 1, 2 and 3, and these were orientated

perpendicular to major structural trends and geological boundaries, including the main landslide

blocks. Line ERT1 was acquired using two arrays (ERT 1A and 1B) in order to sample the entire

length of the landslide deposit, and including the lower non-slipped ground beyond the toe. The

survey design provided for a depth of investigation up to c. 50 m in order to image the shallow and

deep structure of the landslide beyond the estimated depth of the deepest slip surface, based on initial

cross sections and the geomorphological evidence.

Approaches to ERT field surveying are described widely in the literature (e.g. Chambers et al., 2011;

Lapenna et al., 2005), so only a brief explanation is provided here. The ERT field survey was

undertaken during May 2011. ERT data were collected using an AGI SuperSting R8 IP system

attached to stainless steel electrodes via multicore cables. Ground conditions were generally

extremely dry. To reduce contact resistances and improve data quality, each electrode was watered

using a saline solution. Electrode positions were identified using survey tapes extended across the

ground surface; a real-time-kinematic (RTK) GPS measurement, with centimetric accuracy, was then

made for each electrode position, to establish the grid position and elevation of each electrode.

The locations of the four ERT Lines 1A, 1B, 2 and 3 are shown in Fig. 5 as ERT1, ERT2, and ERT3

with lengths of 292.4, 307.6, 289.5 and 184.9 m respectively. (note ERT 1A and 1B are end on and

are depicted as ERT 1 in Figure 5). A dipole-dipole configuration was employed for each of the lines.

The longer lines, Lines 1A, 1B and 2, were surveyed using (along-ground) dipole lengths (*a*) of 5, 10,

15, 20, and 25 m and dipole separations (*na*) of 1*a* to 8*a*. For Line 3, which was a shorter and higher

resolution imaging line, dipole lengths (*a*) of 3, 6, 9, 12, 15, and 18 m, and dipole separations (*na*) of

1*a* to 8*a* were used.

18

361   A summary of the contact resistances and reciprocal error characteristics of the ERT Lines 1A, 1B, 2,

362   and 3 are shown in Table 2. Even with watering, the measured contact resistances were relatively

363   high, with mean resistances of approximately 3,000 Ω, reflecting the very dry conditions at the time.

364   The reciprocal errors do however indicate that reasonable data quality was achieved for most

365   measurements (i.e. >80% of the measured reciprocal pairs had a reciprocal error of <1%). Data points

366   with a reciprocal error of >1% were removed from the data sets, and the reciprocal errors were used to

367   weight the data during the inversion. The misfit errors for ERT Lines 1A, 1B, 2 and 3 were 2.4%,

368   1.1%, 3.4% and 2% respectively indicating good convergence between the model and measured data.

369

370   Table 2. Contact resistance and reciprocal error summary information for ERT Lines 1A, 1B, 2 and 3.

	Number of measurements*	Contact resistance (Ohms)		Fraction (%) of data set below reciprocal error level	
		Mean	SD**	1%	5%
Line 1A	1780	3159.0	4145.9	80.6	95.0
Line 1B	1788	2757.0	1735.6	80.0	93.6
Line 2	1780	3065.0	2656.2	83.3	96.0
Line 3	1980	3175.0	1872.2	87.6	99.1

* Each comprising a reciprocal pair (i.e. a forward and reciprocal measurement)

371   ** standard deviation (SD)

372   It should be noted that ERT models are smoothed images for which resolution decreases with

373   increasing depth of investigation because the model in these regions is less well constrained by the

374   data. The interpretation of 2D ERT imaging data is further complicated by off-line 3D resistivity and

375   topographic variations that violate the 2.5D assumption. Therefore, the ERT images can provide only

376   an approximate guide to the true resistivity and geometry of subsurface features (Olayinka and

377   Yaramanci, 2000; Chambers et al., 2002); and hence, calibration and interpretation using other

378   sources of ground-truth information are highly desirable. This was possible in Zones I and III, where

379   exposure mapping or borehole data were available, but not in Zone II.

380

381   *4.3. Results and interpretation of geophysical imaging (ERT)*

382 The ERT survey Lines 1A, 1B, 2 and 3 (Fig. 6) provide additional information on deep subsurface

383 structure and composition of the landslide mass. The geophysical models for the corresponding ERT

384 Lines 1A, 1B, 2 and 3 are presented in Fig. 6 with borehole and penetrometer test data overlaid to

385 provide information on material characteristics and depths, where available. The low resistivity areas

386 generally correspond with clay-rich materials, such as mudstone lithologies and wet clay soils, and

387 these contrast against more electrically more resistive areas which indicate other materials such as

388 siltstone, sandstone, limestone or free draining dry coarse or very coarse soils. Geological boundaries,

389 depicted in black, are projected into the subsurface and geological units labelled. Oblique formation

390 labels indicate rotated bedding and horizontal labels indicate horizontal bedding. The relationship and

391 distribution of high and low resistivity zones at depth within the main body of the landslide (ERT

392 Lines 1A, 2 and 3) provide evidence of the deep structure where there is no intrusive investigation.

393 Truncation of rectangular high resistivity zones against low resistivity zones in Zone II is interpreted

394 as evidence for rotation and juxtaposition of more resistive beds (e.g. partially or un-saturated

395 sandstone and limestone beds) against low resistivity mudstones. The dashed white lines depict

396 'inferred' positions of the main shear surfaces with arrows indicating direction of slip. In Zone II the

397 geophysical data suggest a c.30 m deep 'upper' slip surface, with an entirely separate 'lower' slip

398 surface. In Zone III the lateral thickness variation in mudflow deposits within the toe can be inferred,

399 with borehole control, from the geophysical model (ERT Line 1, Fig. 6) where the boundary is

400 marked by a sharp transition between lower resistivity zones representing mudstone and higher

401 resistivity, zones representing sandy clay and silt rich materials.

402
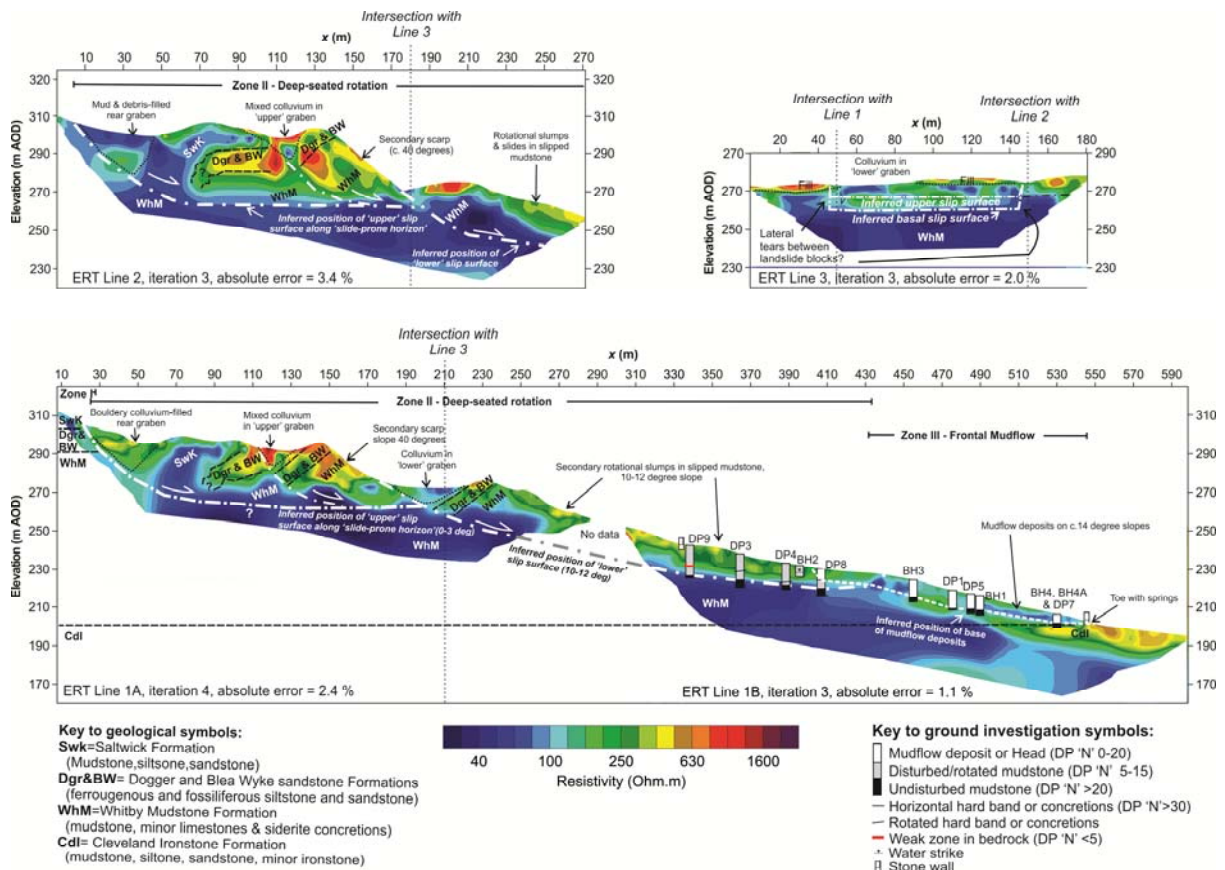
Fig. 6. ERT sections from the Mark Nab landslide with borehole data and preferred interpretation of profile of main slide surface.

5. Slope architecture

An interpretation of the 2D architecture of the slope has been developed by combining the LiDAR digital terrain model (Fig. 4), geology map and geomorphological interpretation (Fig. 5) and the findings of the drilling and geophysics (Fig. 6), following the 'total geological model' approach described by Fookes (1997). The model of the internal architecture and its relation to the bedrock succession is summarised in two cross-sections, Section A and B, in Fig. 7. The location of Section lines A and B are shown in Fig. 5.

21
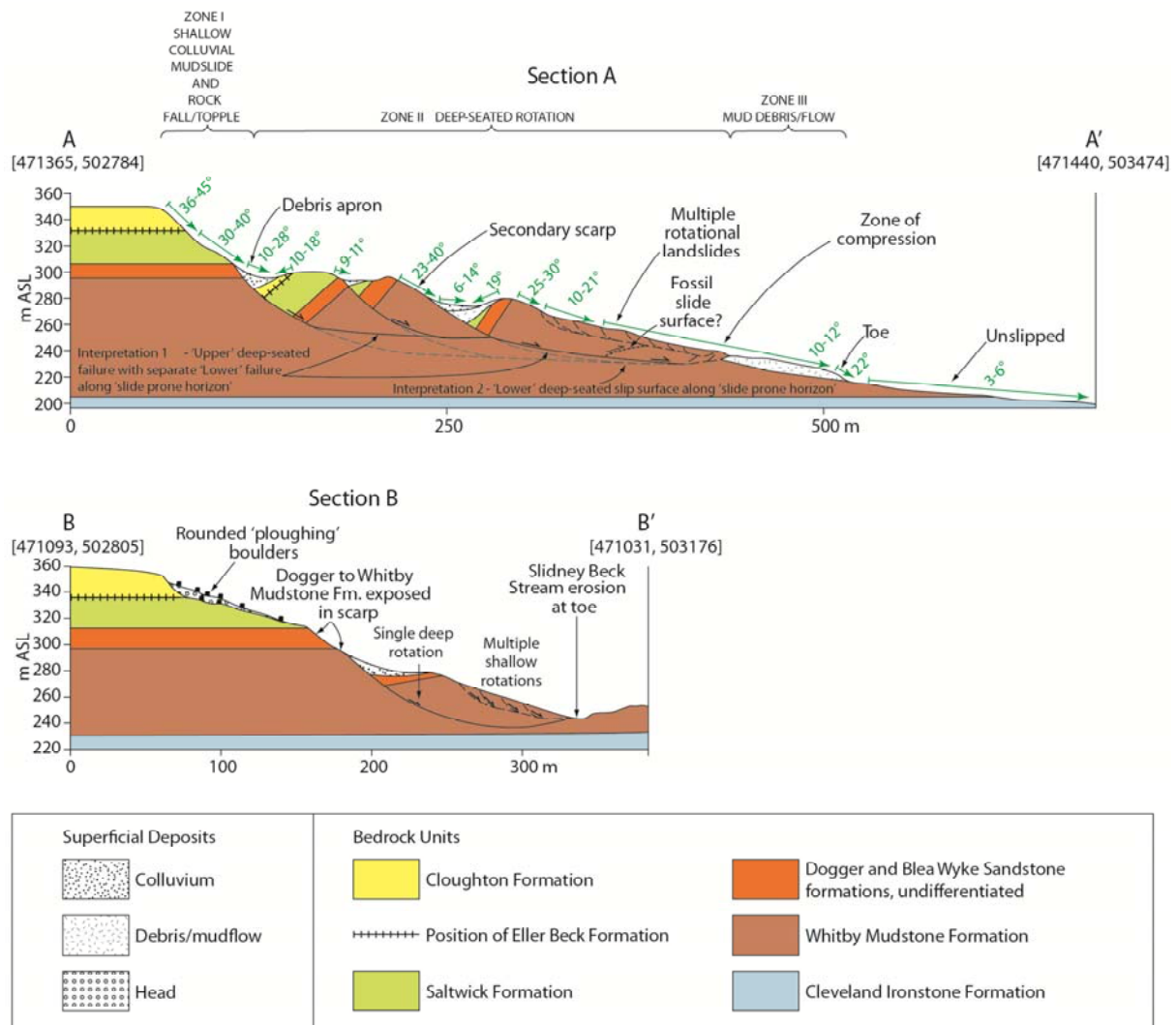
414

415 Fig. 7. Section A: Idealised geological cross section through centre of the Mark Nab landslide

416 showing two possible slip surface geometry interpretations: Interpretation 1 entertains two entirely

417 separated slide surfaces, the 'upper' surface is bedding-controlled and horizontal, the 'lower' is a sub-

418 horizontal non-bedding-controlled surface; while Interpretation 2 considers a multiple rotation with

419 three main blocks and a common basal bedding-controlled slide surface. Zones I–II relate to

420 geomorphological zones described in Fig. 4. Section B: Idealised cross section though the western

421 flank with single compound slide with superficial rotations. Note the location of the cross section

422 lines do not match the location of the geophysical survey lines (see Fig. 5).

423

424 Section A (A–A', Fig. 7) shows an idealised geological cross section through the centre line of the

425 landslide and subsurface relationships between surface morphological features, such as back-tilted

426 sandstone-capped mudstone blocks and key geological marker beds such as the Dogger Member. At

427 the rear of the escarpment (Zone I), the thick horizontally bedded cap rock of well-jointed

428 sedimentary rocks, composed of Dogger Member, Saltwick Formation, Eller Beck Member and

429 predominantly Cloughton Formation, provide a static load on the thick Whitby Mudstone Formation

430 beds. These non-argillaceous units effectively behave as a layered aquifer which along with surface

431 infiltration supply water into the slope. Dilation of existing bedrock joints due to vertical and lateral

432 stress-relief (unloading) has contributed to enhanced bulk porosity and permeability of the cap rock

433 and is an important factor in the hydrogeology.

434 The presence of three large internal blocks within Zone II (deep-seated rotational) suggests that at

435 least two internal slide surfaces are present, and these likely connect with the main slide surface at

436 depth (Fig. 6, Section A). There are several possible interpretations of the slip surface geometry, and

437 the author's two preferred interpretations are labelled in Fig. 6 as Interpretation 1 and 2. The first

438 interpretation involves an 'upper' slip surface, with a c. 30 m deep sub-horizontal planar surface

439 which follows a 'slide prone horizon', as defined by Bromhead and Ibsen (2004), within the Whitby

440 Mudstone (upper beds of the Mulgrave Shale Member), and a completely separate 'lower' slip surface

441 evidenced by the geophysics, which is c. 20 m deep and gently inclined at c. 10–12°. The form of the

442 'lower' slip surface is sub-horizontal, planar or stepped, and cuts through the bedding of theWhitby

443 Mudstone (Mulgrave Shale Member). Both slip surfaces are most likely non-circular.

444 However, an alternative interpretation (Interpretation 2) is also worth consideration. This involves a

445 single deeper-seated non-circular slip surface that cuts through to the base of the Whitby Mudstone

446 Formation. The maximum depth of rupture for this interpretation is c. 50 m, somewhat deeper that

447 interpretation 1, with the slide plane exploiting the full depth of the mudstones of the Mulgrave Shale

448 Member, probably along a landslide prone horizon at or near the base of the formation (bedding plane

449 failure). The simplest geometrical solution supported by geophysical and borehole evidence is

450 Interpretation 1. However, there is some uncertainty about the reliability of the geophysical data at

451 depths beyond 30 m, and so the interpretation of the structural interpretation in Zone II is still largely

452 based on expert judgement.

453 Section B of Fig. 7, which corresponds to B–B' in Fig. 5, is a representation of the western side of the

454 Mark Nab landslide complex. The section depicts the form of the main slide surface at the far western

455 flank as topped by shallow multiple rotations. Erosion of the toe of the landslide mass by Slidney

456 Beck continues to destabilise this part of the Mark Nab landslide system, and this is a process that is

457 actively occurring to the south at the heads of the Great Fryup Valley, and the majority of the other

458 adjacent valleys. Key geomorphological features that are pronounced are the break of slope associated

459 with the relatively resistant Dogger and Blea Wyke sandstone, sharp scarps, and smooth convex

460 slopes found above the 320 m contour line. The upper part of this slope is mantled by soliflucted head

461 deposits that contain weathered rounded sandstone boulders 'ploughing boulders' (Fig. 7 Section B).

462 Erosion of weathered Whitby Mudstone from the rear scarp (e.g. Loc. 12 in Fig. 5) has deposited

463 colluvium onto the head of this slide mass, and although vegetation of the scarp slope has somewhat

464 arrested this erosion process, this area is prone to future instability due to river erosion. Advancement

465 of the conceptual ground model requires drilling rotary boreholes to +60 m in the main body (Zone II)

466 and above the crown. Deeper holes would better constrain the lithostratigraphic unit thicknesses, and

467 provide samples for further materials testing.

468

6. Landslide movement history

6.1. Geomorphological evidence

471 There are no historic records of large-scale movements of the landslide; however, the relative

472 sequence of movements can be inferred from interpretation of the geomorphic and geological

473 evidence. The truncation of periglacial head deposits by the main (rear) back scarp (Figs. 5 and 7B),

474 and the presence of head beneath the mudflow deposits (BH4, Appendix 1), constrain the main

475 movement event to the early-late Holocene times. Preservation of ridge and furrow plough lines in

476 Zone III (Fig. 6) suggests this area has not been active in this area in historic times. However, rotation

477 and dislocation of Whitby Mudstone from the main landslide mass on the western flank (Fig. 7

478 Section B), is evidence for a secondary phase of deep-seated movement after the main event and this

24

479   possibly postdates some of the frontal mudflow activity in Zone III. The minor scarps and benches

480   shown in Zone II (Fig 7 Section B) provide evidence for 'recent' to 'old' rotational slides, driven by

481   toe erosion by Slidney Beck and this process is still intermittently 'active'. Very recent activity is

482   limited to small-scale translational slides in weathered or disturbed mudstone on stream banks and

483   minor rockfall from the sandstone beds exposed along main escarpment cliff and along the banks of

484   drainage gullies (Fig. 5, Locs 4, 12 and 13).

485

486   *6.2. Sediment dating*

487   The frontal mudflow complex (Fig. 4, in Zone III) contains buried palaeosols which were cored and

488   dated to help constrain the age of the latest mudflow events. Inspection of cores during logging of

489   BH4A identified a peat deposit below a mudflow event horizon between 2.74 and 2.90 m b.g.l.

490   (Appendix 1). This soil horizon is composed of olive grey organic silt with pockets of amorphous peat

491   containing fragments of wood and charred material; the upper boundary is sharp indicating erosion by

492   an overriding mudflow event(s). Another horizon containing dark brown peat with scattered rootlets

493   and wood was also proved at a similar depth in BH4, located approx 1 m to the west of BH4A (Fig. 5

494   & Appendix 1). These soils likely preserve deposition and vegetation of shallow surface depressions

495   on the upper surface of a mudflow.

496   Radiocarbon dating methods were used to determine the age of this sediment. Fragments of wood

497   were extracted during examination using clean gloves and tools to minimise contamination.

498   Precautions were also taken during percussive drilling to minimise hydrocarbon contamination (duck

499   oil). The sediment samples were stored horizontally in a humidity and temperature controlled fridge at

500   4°C for c. 6 months at BGS Keyworth prior to logging and sampling. Three of the fragments of wood,

501   extracted from various depths between 2.84 to 2.89 m in BH4A, were analysed for age determination

502   using Accelerator Mass Spectrometry (AMS) techniques by Beta Analytic (Beta Nos 343215, 343216,

503   343217). Samples were analysed to ISO 17025 standards, and were first pre-treated using the

504   acid/alkali/acid method. The results of the AMS analysis are shown in Table 3.

505

506   Table 3. Radiocarbon-dated samples from the Mark Nab landslide mudflow cores.

Core	Depth (m)	OS Grid reference (x,y,)	Sample type and pre-treatment	Lab. ID number	Measured Age (BP)	13C/12C o/oo	Conventional ^{14}C age (BP)	2 SIGMA CALIBRATION
BH4A	2.850-2.900	471566, 503341	Charred material: acid/alkali/acid	Beta-343217	2240±30	-23.0	2270± 30	Cal BC 400 to 350 (Cal BP 2350 to 2300)/Cal BC 290 to 230 (Cal BP 2240 to 2180)/Cal BC 220 to 210 (Cal BP 2170 to 2160)
BH4A	2.840	471566, 503341	Charred material: acid/alkali/acid	Beta-343216	2340±30	-23.2	2370±30	Cal BC 510 to 390 (Cal BP 2460 to 2340)
BH4A	2.870	471566, 503341	Charred material: acid/alkali/acid	Beta-343215	2340±30	-26.2	2320±30	Cal BC 400 to 380 (Cal BP 2360 to 2330)

507

508   These dates constrain the latest mudflow event in BH4A to after 2270 yrs BP. The earliest date of the

509   buried palaeosol coincides with a period of climatic deterioration to a wetter climate, but also major

510   woodland clearance by early Iron Age people, as indicated for example by pollen records from the

511   nearby Fen Bogs site (Simmons et al., 1993; Innes et al., 1999). This late-Holocene erosion event

512   corroborates other records from wetlands formed behind landslides in the North York Moors at

513   Gormire Lake, St Helena and Blakey, where a link between erosion and deforestation has been

514   suggested by Innes et al. (1999).

515

516   7. Landslide trigger factors and mechanisms of failure

517   *7.1. Slope stability models*

518   A set of slope stability models were developed to quantitatively test the conceptual ground model and

519   explore the initial landslide trigger factors and assess the current day stability state. The geotechnical

520   property values used in the stability models are provided in Table 4. The values were estimated

521   values, based mainly on the BGS's geotechnical database for the Lias Group (Hobbs et al., 2005) and

522   the general literature (Reeves et al., 2006). A small number of geotechnical tests (ring shear and shear

523   box) were carried out on samples of Whitby Mudstone Formation collected from the landslide deposit

524 itself (shear zone exposed at head of gully near Loc 4, Fig. 5.) and other samples collected from

525 another landslide shear zone exposed at river level at nearby East Arnecliff Wood. These data were

526 not used directly but were used to inform an expert judgement based estimate of the residual shear

527 strength of the Whitby Mudstone at the Nark Nab landslide site. The density and porosity data were

528 taken mainly from the BGS's geotechnical database. Two main slope scenarios were modelled: i) a

529 pre-failure slope, and ii) the present day 'post-failure' slope.

530

531 Table 4. Geotechnical property values used for slope stability models (after Hobbs et al., 2005;

532 Reeves et al., 2006; Hobbs and Boon, 2013). c': effective cohesion ; ϕ:effective angle of internal

533 friction.

Geological layer (lithology)	Layer thickness (m)	Saturated density (kg m^{-3})	Dry density (kg m^{-3})	Porosity, n (%)	Pre-slip 'peak'		Post-slip 'residual'	
					c' MPa	ϕ· degr.	c' MPa	ϕ·$_r$ (degr.)
Cloughton Formation (Sst) including Eller Beck Formation	20	2450	2300	0.15	0.30	35	0.0	35
Saltwick Formation (Sst/Slst/Mst)	25	2350	2200	0.15	0.20	25	0.0	25
Dogger & Blea Wyke Formations (Sst/Slst)	10	2300	2100	0.20	0.11	20	0.0	20
Whitby Mudstone Formation (Mst)	201	2060	1710	0.35	0.015	26	0.0	10
Cleveland Ironstone Formation (Slst/Mst/Irnst)	infinite	2060	1710	0.35	0.5	30	0.5	30

534

535 *7.2. Pre-failure slope scenarios*

536 The model was used to perform a 'back-analysis' to investigate the sensitivity of the paraglacial

537 Jurassic Escarpment to various environmental trigger factors, including:

538 (1) Glacial buttressing and loss of that lateral support (de-buttressing)

539 (2) Presence of a pro-glacial lake

540 (3) Groundwater level rise after deglaciation

541

542   The model variables chosen to represent these primary factors were: slope angle, groundwater level,

543   and surface water level, respectively. The pre-failure slope analyses used two approaches: 'finite

544   element' using FLACslope (version 7) and 'limit-equilibrium' using Galena (version 6). The results

545   from finite element modelling were, where appropriate, used to inform the geometry of the slip

546   surface defined in the limit-equilibrium model. Further details of the analyses methods and results are

547   provided in Hobbs and Boon (2013). The surface profile was based on a structural reconstruction of

548   the cross section in Fig. 6A, which assumes a 43° planar slope.

549

550   *7.3. Glacial buttressing*

551   To investigate the potential effect of glacial buttressing on the sequence of slope deformation we

552   considered two simple models:

553   i) Ice buttressed: over steepened slope, 80 m high, with ice buttressing up to the 270 m contour line.

554   ii) Non-buttressed: over steepened slope, 125 m high, no ice buttressing.

555   Both scenarios were modelled in FLAC using the same geological unit thicknesses (Fig 8A) and

556   'peak' strength properties (Table 4). The water table in model (i) was assumed to be deep, assuming

557   no free water and deep permafrost conditions, whereas the water table in model (ii) assumes a shallow

558   water table and re-establishment of the regional water table and potential for excess pore pressure

559   build up in the slope.

560   The FLAC modelling results are shown in Fig. 8B,C. Fig. 8B shows the over steepened 'buttressed'

561   slope is inherently unstable (*FoS* of 0.95) and prone to failure, but with shallow movement occurring

562   as minor shallow rotation affecting only the Whitby Mudstone and Dogger units. This result supports

563   the idea of an initial 'upper' slope failure (as implied by 'Interpretation 1'; Fig. 6A). The results of

564   model (ii) in Fig. 8C, shows the slope is also unstable when glacial de-buttressing has occurred, but

565   the failure mode is significantly different from that of the buttressed slope stability model (i), with a

566   deep-seated rotation affecting the full slope in Fig. 8C. One key limitation of this slope modelling

567   method is that model (i) substitutes the ice mass for a Whitby Mudstone mass due to software

568   limitations. Therefore, model (i) is unlikely to produce a deeper basal failure mode (similar to

569   Interpretation 2 in Fig. 6). However, a deep-seated bedding-controlled failure with a basal slip surface

570   geometry which daylights within the ice mass, similar to Interpretation 2 Fig. 6A, is also a feasible

571   failure mechanism.

572
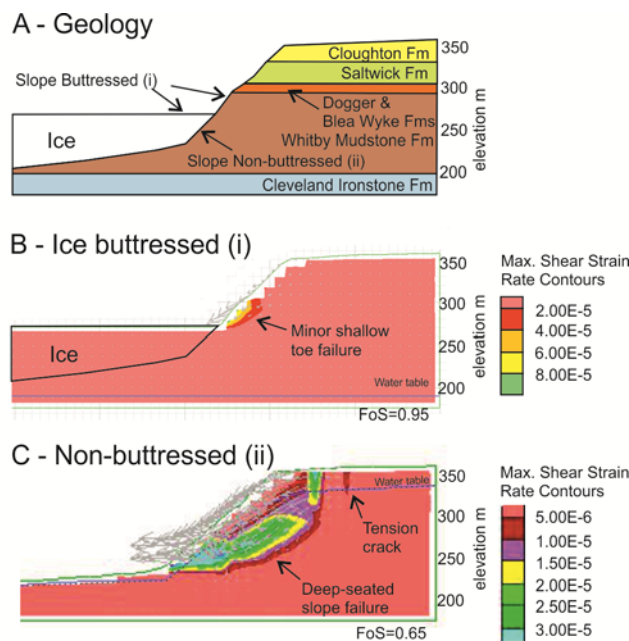
574   Fig. 8. Results of FLAC slope stability modeling. A) Geological layers. Properties given in Table 4.

575   Note: Ice mass is substituted for Whitby Mudstone Formation properties due to software limitations.

576   B) Results for a glacially buttressed slope scenario. C: Results for a glacially de-buttressed slope

577   scenario.

578   *7.4. Model sensitivity*

579   One assumption in the models is that the para-glacial slope was c. 43°. This slope angle is based on

580   cross section reconstruction and so there is a lot of uncertainty in the pre failure slope angle. To

581   investigate the sensitivity of the stability models to this uncertainty , and to better understand the

582   general relationship between slope angle and stability condition across the region, we modelled a

583   range of generic Whitby Mudstone Formation slopes using FLAC. We use 'peak' strength properties

29

584 (Table 4) and assume the formation is 90 m thick. The results are plotted in Fig. 9A, which shows that

585 the Jurassic Escarpment becomes increasingly unstable as slope angle increases. This result is not

586 surprising; however, the relationship suggests that if a 90 m thick Whitby Mudstone Formation slope

587 exceeds a critical angle of c. 22° the failure mode is more likely to favour deep-seated rotational

588 sliding over a translation sliding mode. The slide plane exploits 'landslide prone horizons' entirely

589 within the Whitby Mudstone Formation and the primary shear surface daylights at the base of the

590 escarpment (in a toe failure), above the Cleveland Ironstone Formation. To validate the model result

591 with empirical data, slope angles of failed and non-failed slopes in Great Fryup Dale were measured

592 remotely in GeoVisionary using a slope model derived from the 0.25 m resolution LiDAR data (Fig.

593 4). Using this approach we find that deep-seated landslides tend only to be found on the Jurassic

594 escarpment when the average slope angle exceeds c. 21°. This empirical method not only provides a

595 useful 'sense check' on the assumptions made in the stability modelling, but also provides an

596 improved understanding and a critical slope angle cut off which could be applied for regional

597 landslide susceptibility mapping purposes.

598 *FoS* for a conceptual pre-slipped Whitby Mudstone slope (i) is 0.8, suggesting that without additional

599 lateral support (i.e. glacial buttressing) these slope would not have stood up on its own at c. 43°.

600 Following this logic it is highly plausible that an initial 'upper' slope failure initiated in the upper part

601 of the escapement (a 'slope failure') while the glacier was still providing some lateral support (i.e.

602 paraglacial failure). The slope may have even started to relax due to lateral unloading during valley

603 glaciation phases, with dilation of pre-existing discontinuities (e.g. Joints, faults, fractures) which

604 would have increased the secondary hydraulic permeability of the rock mass. The combined effects of

605 these geological processes would have preconditioned the slope for a further 'lower' failure as the ice

606 mass reduced in volume. We have represented this rock mass dilation effect in our stability models by

607 addition of a tension crack 10 m behind the crown. However, the presence of frozen ground under

608 permafrost conditions could also have increased the shear strength of the near surface slope materials,

609 delaying development of a shallower failure mechanism in favour of a deeper-seated slope failure

610   which propagates beneath the frozen crust. This failure mechanism could account for the existence of

611   large intact blocks preserved in Zone II.

612   Although the pre-slip stability model (Fig. 8A) results presented thus far lend support to a deep-seated

613   rotational mode of failure during a partial glacial de-buttressing phase, other potential trigger factors,

614   such as the reported pro-glacial lake in Eskdale and a post glacial rise in regional groundwater levels,

615   may also have contributed to the hillslope instability along the non-glaciated parts of the escarpment

616   and in other regions south of the Devensian limit, such as the Cotswolds. These two additional trigger

617   factors were investigated using modified slope stability models and the methods and results are briefly

618   described in the following subsection.

619
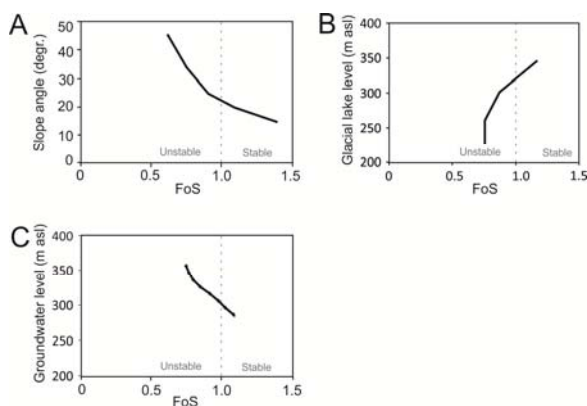
621   Fig. 9. Plots showing the results of slope stability model sensitivity analysis of key physical factors

622   for Whitby Mudstone Formation slopes: A) relationship between slope angle and *FoS*; B) glacial-lake

623   level and *FoS*; and C) relationship between *FoS* and regional groundwater level. (A) and (B) assume a

624   deep-seated non-circular rotational failure mode on a 43° hillslope in horizontally-bedded Whitby

625   Mudstone Formation mudstone.

626

627   *7.5. Glacial lake drawdown scenario*

628   Kendall (1902) proposed the Esk valley was once flooded by a pro-glacial lake, Lake Eskdale, which

629   reached a maximum height of 225 m aOD (Kendall, 1902; Radge, 1939; Gregory 1962a,b; Kent et al.,

630   1980; Murton and Murton, 2011). If this lake really did exist, the lake water would partially filled

631 Great Fryup Dale and the adjacent valleys. The effect of a changing water body level on the stability

632 of the pre-slip Jurassic Escarpment was modelled by varying the level of the water table in the

633 stability model.

634 The results, plotted as the relationship between lake level and stability state (FoS) in Fig. 9B, indicate

635 that a rising lake level would have promoted stability, but that a rapid lowering of the lake level, while

636 the slope is still in a saturated state, would have promoted instability.

637

638 *7.6. Groundwater rebound scenario*

639 A similar reduction in stability is also achieved by raising the regional groundwater level, so draining

640 of a pro-glacial lake would probably not have been required to trigger the initial main failure as the

641 slope was already likely metastable anyway. The climatic amelioration at the start of the Holocene

642 would have seen re-establishment of the surface drainage network and a rise in regional groundwater

643 levels. This is evidenced by formation of sapping erosion related landforms such as the Hole of

644 Horcum which is reputed to have formed shortly after the LGM (Cooper, 2007). To test the sensitivity

645 of an oversteepended deglaciated slope to rising groundwater levels we back-analysed a Whitby

646 Mudstone slope using the reconstructed pre-slip hillslope geometry of 43° and peak strength values

647 (Table 4). The groundwater level was raised in increments of 10 m to simulate rising groundwater

648 conditions, under long term 'drained' effective stress pore water conditions. The model results

649 summarised in Fig. 9C indicate that a rise in groundwater level significantly reduces the stability of

650 the Jurassic escarpment slope. The model is also very sensitive to slope angle (Fig 9Aa). The stability

651 model results from Hobbs and Boon (2013) show that a deep-seated rotational failure mode is

652 favoured when groundwater level rises above around 303 m aOD. When groundwater level reaches

653 this elevation the sandstone cap rock (Dogger Formation) would have seemingly become fully

654 saturated and started to behave like an aquifer by providing water into the landslide prone Whitby

655 Mudstone Formation unit below and increased its load, hence promoting instability.

656

7.7. Likely trigger mechanisms of UK Jurassic escarpment landslides

The most feasible primary trigger mechanism for the initial Mark Nab landslide is loss of lateral support due to over steepening of the slope by glacial erosion and de-butressing, although groundwater rise likely also played a role. Subsequent increases in effective rainfall and stream down-cutting and erosion likely drove secondary movements, further block disruption, and initiated subsequent first time failures at the heads of incised valleys. Seismic and rainfall triggering were also considered, but not modelled. More widely, the combined roles of (i) glacial de-buttressing, as described by McColl and Davies (2013); and (ii) bedding-controlled failure, similar to that described in SE England by Bromhead and Ibsen (2004), and (iii) regional groundwater rise, likely triggered and drove landslide activity along glaciated and non-glaciated Jurassic slopes in Britain. In the deep, supposedly non-glaciated (during the Devensian) incised moorland valleys to the south, such as Rosedale, it is possible that first-time failures occurred due to over-steepening that occurred during earlier valley glaciation, and reactivation occurred under rising groundwater level conditions, although more investigation is needed.

Reconstruction of the slope profile at Mark Nab also provides a new estimate of recession rate for the Jurassic Escarpment in glaciated valleys in Northern Britain through the Holocene; we estimate between 0.01 and 0.005 m yr^{-1} of recession to have occurred since the LGM, mainly controlled by mass movement processes. This rate assumes the main phase of landslide-driven erosion initiated c. 13,000 yrs BP, at the end of the Late Devensian, although more precise dating of the main failure would help constrain these estimates.

7.8. Current stability state

The residual stability of the majority of relict landslides in the UK is largely unknown, and although they are generally considered dormant or inactive (Jones and Lee, 1994), they have been known to reactivate and cause damage (e.g. Fish et al., 2006). Effective assessment of relict slopes requires appropriate site investigation and a ground model.

683   We used the Galina software package to model the stability state of the 'present day' slope using the

684   current topographic profile determined from the 5-m NextMap, and 'residual' shear strength values

685   for the landslide-prone Whitby Mudstone Formation (Table 4). We also considered sensitivity of the

686   model to different slip plane geometry and modelled the stability condition using the both the shallow

687   and deep slip plane geometries proposed in 'Interpretation 1' and 'Interpretation 2' of Fig. 7 Section

688   A, respectively.

689   The Sarma non-vertical (multi) slice, non-circular analyses were used for all Galena models. The

690   'residual' strength value (ϕ'_r) for the Whitby Mudstone Formation was increased from the laboratory

691   measured value of 9° to 10° to account for the fact that the clay is unlikely to be at fully remoulded

692   strength at the field scale due to inclusion of lithorelicts, discontinuity roughness effects, and possible

693   added cohesion provided by secondary crystallisation along ancient inactive shear surfaces.

694   The results of the Interpretation 1 model (involving an 'upper' and 'lower' slip surface geometry

695   based on Fig. 7A), indicate the 'upper' landslide mass is currently stable ($FoS = 2.71$), and the

696   separate 'lower' slide mass of Interpretation 1 is also stable ($FoS = 1.42$). If we assume the both slip

697   surfaces are connected and the landslide mass behaves as one coherent mass the slope is also

698   seemingly stable ($FoS = 1.85$). There was no field-based evidence to suggest the main landslide

699   masses are currently unstable, other than minor failures along gulley slopes, and the stability

700   modelling strengthens the notion that the slope as globally 'dormant'. However, the stability of the

701   'upper' mass would decrease if the 'lower' mass were to move, as the latter provides some clear

702   buttressing, these interdependencies highlight the dynamic nature of these landslide systems and it

703   seems likely that complex and delicate physical feedbacks are still in operation within these relict

704   slopes.

705   In terms of landslide activity state using the terminology of Jones and Lee (1994), the evidence from

706   the dating of mudflows in Zone III suggests they are 'Dormant' rather than 'Inactive – Ancient'

707   implying Zone III areas at this site, and similar Zone III type slopes elsewhere in the region, are most

708   prone to reactivation by extreme environmental conditions such as increased effective rainfall.

709

710 *7.9. Model uncertainty and sensitivity*

711 *7.9.1. Current day slope*

712 There is uncertainty in the 'current day' stability model, which relies heavily on assumptions about

713 the geometry of the slide planes(s). The slide plane geometry is more certain where there is drilling

714 and geophysics data (Zone I). There is some uncertainty in the 'post slip–residual' model input values

715 (Table 4) which were limited to lab-scale test results so these may not accurately reflect field-scale

716 values. Although some provision was made for this, by increasing residual strength value slightly

717 from 9° to 10°, the material and mass strength will likely vary at the field-scale due to a variety of

718 multi-scale effects and processes, including: variability in clay content and type, re-consolidation

719 (Gibo et al., 2002), large-scale 3D internal friction effects between landslide blocks (Morgenstern,

720 1995), external friction effects along mudstone landslide boundaries (e.g. Massey et al., 2013), and

721 secondary mineralisation increasing shear resistance (adding cohesion). Another source of error in the

722 stability models is the accuracy of the position of the water table, and the assumption this is static. In

723 the 'current day' slope model the water table is assumed planar with its depth informed by peizometer

724 data from BH2, although this level is unlikely to be uniform across the slope, as the occurrence of

725 springs testifies.

726

727 *7.9.2. Pre-slide slope*

728 The pre-slide slope stability models have some major limitations, for example, the pre-slipped slope

729 profile, groundwater levels and pre-slip slip surface geometry are estimates, constrained by limited

730 ground monitoring data, as previously discussed. The pre-slide slope stability model is very sensitive

731 to slope angle, as shown from the sensitivity analysis of slope angle in Fig. 9A. The geotechnical

732 values (Table 4) are also largely estimates based on values from the literature and some limited shear

733 strength testing from on-site and nearby site materials. Nevertheless, back-analysis using slope

734 stability modelling techniques does offer a useful tool to test our understanding of plausible failure

735 mechanisms in ancient landslides, and informs the current day regional hazard and sensitivity of the

736   system to environmental and anthropogenic perturbations. To reduce the uncertainties in the ground

737   model, and the stability models developed from it, deep drilling is required with groundwater

738   monitoring, materials testing, mineralogical studies, and further geophysics (e.g. passive and active

739   seismic).

740

8. Conclusions

742   A combination of geological, geomorphological, geophysical, dating, and stability modelling

743   techniques have been applied here to reconstruct the 2D architecture and failure mechanism of a relict

744   landslide on the Jurassic Escarpment in Northern England. This paper provides the basis for a

745   preliminary ground model for the Mark Nab slope and the numerous other large, deep-seated bedrock

746   landslides typically found across the North York Moors region. The study shows that the large slope

747   failures are typically developed in weak mudstone lithology of the Lower Jurassic mudstones (Whitby

748   Mudstone Formation) and the principal failure mechanism is geologically controlled by the thickness

749   of the mudstone and the presence of bedding controlled failures along 'slide-prone horizons'.

750   Geomorphological evidence and new radiocarbon dating of sediment provides new understanding of

751   the landslide movement history, and this knowledge helps inform expert based landslide hazard

752   assessment in the region. The study includes the first application of the ERT geophysical technique to

753   image a deep-seated landslide in Jurassic rocks in the Cleveland Basin. The combined approach,

754   where ERT is calibrated with borehole data and detailed geological mapping, proved crucial in the

755   assessment of the landslide deposit volume, 3D internal architecture and depth of principal slip

756   surfaces. Static slope stability modelling (non-dynamic) suggests that the slope most likely initially

757   failed in response to glacial over steepening and de-buttressing. However, groundwater rise is also a

758   contributing factor to instability in the region, and may have triggered and reactivated the large

759   landslides in the adjacent non-glaciated valleys, such as Rosedale. Slope reconstruction provides new

760   recession rate estimations for the North Yorkshire Jurassic Escarpment. Although currently inactive

761   and dormant, the frontal mudflow complexe has at Mark Nab has been active within the last 2700

762 years BP, and this and similar slopes are moderately prone to becoming unstable again under future

763 wetter climates. These mudflow systems can be easily recognised and mapped using modern high

764 resolution LiDAR data to improve landslide hazard maps and models. Importantly, this slope and

765 other similar ones are also vulnerable to renewed instability caused by adverse anthropogenic activity,

766 drainage alteration or major civil engineering works. The combined geomorphological and

767 geophysical approach described through this case study will be of interest to hazard geologists and

768 engineering geologists working on landslide problems in similar geological settings, including other

769 UK Jurassic escarpments, and overseas. The paper is also relevant to those involved with or planning

770 landslide hazard and risk studies in high latitude regions currently undergoing active de-glaciation.

771

783

References

785

786 Anon. 1972. The preparation of maps and plans in terms of engineering geology. Quarterly Journal of

787 Engineering Geology 5, 297-367.

788

789 Anon, 1995. The description and classification of weathered rocks for engineering purposes. Engineering Group

790 of the Geological Society Working Party report. *Quarterly Journal of Engineering Geology*, Vol. 28, 207–

791 242.2)

792

793 British Standards Institution. 1999. BSI 5930:1999 Code of Practice for Site Investigations, incorporating

794 Amendments 1 and 2. British Standards Institution, London.

795

796 Barron, A. J. M., Lott, G.K., Riding, J.B. 2012. Stratigraphical framework for the Middle Jurassic strata of Great

797 Britain and the adjoining continental shelf. *British Geological Survey Research Report* RR/11/06. 187pp.

798

799 Bromhead, E.N., Ibsen, M.-L. 2004. Bedding-contolled coastal landslides in Southeast Britain between

800 Axmouth and the Thames Estuary. Landslides. 1:131-141.

801

802 Chambers, J. E., Ogilvy, R. D., Kuras, O ., Cripps, J. C. & Meldrum, P. I. 2002. 3D electrical imaging of known

803 targets at a controlled environmental test site. Environmental Geology 41, 690-704.

804

805 Chambers, J. E., Wilkinson, P. B., Kuras, O., Ford, J. R., Gunn, D. A., Meldrum, P. I., Pennington, C. V. L.,

806 Weller, A. L., Hobbs, P. R. N. & Ogilvy, R. D. 2011. Three-dimensional geophysical anatomy of an active

807 landslide in Lias Group mudrocks, Cleveland Basin, UK. Geomorphology 125, 472-484.

808

809 Chiverrell, R.C., Thomas, G.S.P. 2010. Extent and timing of the Last Glacial Maximum (LGM) in Britain and

810 Ireland: a review. J. Quaternary Sci. 25, 535-549.

811

812 Cooper, R.G. 2007. Mass Movements in Great Britian. Geological Conservation Review Series, No. 33. Joint

813 Nature Conservation Committee, Peterborough.

814

815 Cox. B. M., Sumbler. M. G., Ivimey-Cook. H.C. 1999. A formational framework for the Lower Jurassic of

816 England and Wales (onshore area). British Geological Survey Research Report RR/99/01. British Geological

817 Survey.

818

819   Cruden, D. M., Varnes, D.J., 1996. Landslide types and processes. In *Special Report 247: Landslides:*

820   *Investigation and Mitigation*, Transportation Research Board, Washington D.C.

821

822   Fell, R., Corominas, J., Bonnard, C., Cascini, L., Leroi, E. and Savage, W. Z. 2008. Guidelines for landslide

823   susceptibility, hazard and risk zoning for land use planning. Engineering Geology 102. pp85-98

824

825   Fish, P. R., Moore, R. & Carey, J.M. 2006. Landslide geomorphology of Cayton Bay, North Yorkshire, UK.

826   Proceedings of the Yorkshire Geological Society 56, 5-14.

827

828   Fookes, P. G. 1997. Geology for Engineers: the Geological Model, Prediction and Performance. Quarterly

829   Journal of Engineering Geology and Hydrogeology 30, 293-424.

830

831   Fox - Strangways, C.F., Reid, C., & Barrow, G., 1885. The Geology of Eskdale, Rosedale & etc. Explaination

832   of quarter-sheet 96 N.E. New Series Sheet 43. Memoirs of the Geological Survey. 56pp.

833

834   Gibo, S., Egashira, K., Ohtsubo, M., Nakamura, S. 2002. Strength recovery from residual state in reactivated

835   landslides. Geotechnique. 52, No. 9, 683-686.

836

837   Gregory, K, J. 1962a. Contributions to the geomorphology of the North York Moors. (Unpublished PhD thesis).

838

839   Gregory, K.J. 1962b. The deglaciation of Eastern Eskdale, Yorkshire. 1962. Proceedings of the Yorkshire

840   Geological Society 33, 363-380.

841

842   Griffiths. J. S. (eds). 2002. Mapping in Engineering Geology. GSL Key Issues in Earth Sciences. Geological

843   Society of London. pp294.

844

845 Hobbs, P.R.N., Entwisle, D.C., Northmore, K.J., Sumbler, M.G., Jones, L.D., Kemp, S., Self, S., Barron, M. and

846 Meakin, J.L. 2005. Engineering Geology of British Rocks & Soils: The Lias Group. British Geological Survey,

847 Internal Report No. IR/05/008.

848

849 Hobbs, P.R.N., Boon, D.P. 2013. Great Fryup landslide: slope stability analyses. British Geological Survey

850 Internal Report IR/13/002. British Geological Survey, Nottingham.

851

852 Holliday, D. W., Howard, A. S., Pattison. 1992. Sheet 43 Egton (Eskdale and Farndale) solid and drift edition.

853 British Geological Survey. HMSO.

854

855 Howard, A.S. 1985. Lithostraigraphy of the Staithes Sandstone and Cleveland Ironstone formations (Lower

856 Jurassic) of north-east Yorkshire. Proceedings of the Yorkshire Geological Society. Vol. 45, 261-275.

857

858 Innes, J.B. 1999. *In* Bridgland, D.R., Horton. B.P. & Innes, J.B. (eds) 1999. The Quaternary of North-East

859 England. Field Guide, Quaternary Research Association, London. p21-34.

860

861 Innes, J.B., Rutherford, M.M., O'Brien, C.E., Bridgland, D.R., Mitchell, W.A., Long, A.J. 2009. Late Devensian

862 environments in the Vale of Mowbray, North Yorkshire, UK: evidence from palynology. Proceedings of the

863 Geologists' Association 120, 199-208.

864

865 Johnson. R., Fish, P. 2012. Reactivation of the coastal landslide system at Cayton Bay, North Yorkshire, UK.

866 Proceedings of the Yorkshire Geological Society 59, 77-89.

867

868 Jones, D.K.C., Lee, E.M. 1994. Landslides and landsliding in Great Britain. HMSO, London.

869

870 Jones. R. L. 1977. Late Quaternary vegitational history of the North York Moors. V. The Cleveland dales.

871 Journal of Biogeography 4, 353-362.

872

873   Jones, R. L. 1999. In: Bridgland, D.R., Horton. B.P. & Innes, J.B. (eds) 1999. The Quaternary of North-East

874   England. Field Guide, Quaternary Research Association, London. 204pp

875

876   Jongmans, D., Garambois, S. 2007. Geophysical investigation of landslides : a review. Bulletin De La Societe

877   Geologique De France 178, 101-112.

878

879   Kendall, P.F.,1902. A system of glacial lakes in the Cleveland Hills. Quarterly Journal of the Geological Society

880   58, 471-571.

881

882   Kent, P., Wilson, V., Gaunt, G.D., 1980. British Regional Geology Eastern England from the Tees to The Wash.

883   Second ed. Institute of Geological Sciences. HMSO.

884

885   Lapenna, V., Lorenzo, P., Perrone, A., Piscitelli, S., Rizzo, E. & Sdao, F. 2005. 2D electrical resistivity imaging

886   of some complex landslides in the Lucanian Apennine chain, southern Italy. Geophysics 70, B11-B18.

887

888   Marsay, B. 2010. "T'ills was Fallin Down" The Great Landslip of 1872. Bilsdale Study Group. pp82

889

890   Massey, C.I., Petley, D.N. McSaveney, M.J. 2013. Patters of movement in reactivated landslides. Engineering

891   Geology 159, 1-19.

892

893   McColl, S.T. and Davies, T.H.R. 2013. Large ice-contact slope movements: glacial buttressing, deformation and

894   erosion. Earth Surf. Process. Landforms 23, 1102-1115.

895

896   Merritt, A. J., Chambers, J.E., Murphy, W., Wilkinson, P.B., West, L.J., Gunn, D.G., Meldrum, P.I., Kirkham,

897   M., Dixon, N. 2013. 3D ground model development for an active landslide in Lias mudrocks using geophysical,

898   remote sensing and geotechnical methods. Journal of the International Consortium on Landslides. DOI

899   10.1007/s10346-013-0409-1.

900

901   Morgenstern, N.R., 1995. Keynote paper: the role of analysis in the evaluation of slope stability. In: Bell (Ed.),

902   Landslides. Balkema, Rotterdam.

903

904   Murton, D.K. and Murton, J.B. 2011. Middle and Late Pleistocene glacial lakes of lowland Britain and the

905   southern North Sea Basin. Quaternary International 260, 115-142.

906

907   Olayinka, A. I. & Yaramanci, U. 2000. Assessment of the reliability of 2D inversion of apparent resistivity data.

908   Geophysical Prospecting 48, 293-316.

909

910   Powell, J.H ., Cooper, A. H., Benfield, A C. 1992. Geology of the country around Thirsk. Memoir of the British

911   Geological Survey, Sheet 52 (England and Wales).

912

913   Powell, J.H. 2010. Jurassic sedimentation in the Cleveland Basin: a review. Proceedings of the Yorkshire

914   Geological Society 58, 21-72.

915

916   Radge, G.W. 1939. The glaciation of North Cleveland. Proceedings of the Yorkshire Geological Survey 24,

917   190-205.

918

919   Reeves, G.M., Sims, I., Cripps, J.C. (Eds.), 2006. Clay Materials Used in Construction. The Geological Society,

920   Engineering Geology Special Publication. No. 21.

921

922   Schuster, R. L., and Highland. L. M. 2001. Socioeconomic and environmental impacts of landslides in the

923   Western Hemisphere. U.S. Dept. of the Interior, U.S. Geological Survey Open File Report 01-0276.

924

925   Senior, J. and Rose, J. 1994. The Jurassic, Tertiary and Quaternary around Great Ayton and Roseberry Topping,

926   Cleveland Hills, 11. In: Scrutton, C. (ed.) Yorkshire Rocks and Landscape - A Field Guide. Yorkshire

927   Geological Society.

928

929   Simmons, I. G., Atherden, M.A., Cloutman, E.W., Cundill, P.R., Innes, J.B., Jones, R.L. 1993. Prehistoric

930   environments. In: Spratt, D.A. (ed.) Prehistoric and Roman Archaeology of North-East Yorkshire. Council for

931   British Archaeology Research Report 87, BAR British Series 104, Council for British Archaeology, London,

932   15-50.

933

934   Waltham, A., Forster, A. 1999. Man as geological agent. GEOLOGY TODAY, November–December 1999 vol

935   217. Blackwell Science Ltd.

936

937   Young, T.P. 1994. The Blea Wyke Sandstone Formation (Jurassic, Toarcian) of Rosedale, North Yorkshire, UK.

938   Proceedings of the Yorkshire Geological Society 50, 129-142.